

Resonant Optical Second Harmonic Generation and Mixing

A. ASHKIN, MEMBER, IEEE, G. D. BOYD, MEMBER, IEEE, AND J. M. DZIEDZIC, MEMBER, IEEE

Abstract—Experimental and theoretical results are described on the enhancement of optical second harmonic generation (SHG) and mixing in KDP by the use of optical resonance. Both resonance of the harmonic and of the fundamental are considered. Large enhancements are possible for resonators with low loss. Using a plano-concave harmonic resonator containing 1.23 cm of KDP, the authors achieved a loss < 4 percent per pass. This resulted in an enhancement of ~ 500 times the harmonic power internal to the resonator and ~ 10 times external to the resonator. When resonating, the fundamental enhancements of ~ 5 were observed.

The theory includes the effect of double refraction. This results in a coupling coefficient of the generated harmonic power to the transverse modes of the harmonic resonator. The experimental results are in substantial agreement with the theory.

I. INTRODUCTION

THIS PAPER DEALS with the use of optical resonance to enhance the efficiency of optical second harmonic generation (SHG) and mixing. Since the first observation of SHG by Franken, Hill, Peters, and Weinreich (FHPW) [1], there has been considerable progress in understanding the factors contributing to efficient conversion of fundamental to harmonic, and to frequency mixing in general. Aside from finding new materials with larger nonlinear coefficients, increases in efficiency at fixed fundamental power have come about by increasing the interaction length. For a given fundamental frequency beam, this is the maximum length of crystal in which the polarization at the harmonic frequency radiates cooperatively.

The first observations of SHG [1] were made with pulsed ruby lasers and a nonlinear crystal in which the dispersion in velocity between the fundamental light and the harmonic light limited the interaction length to about 14 microns. The introduction of phase-matching techniques [2], [3] in KDP permitted a considerable increase in the interaction length. In the limit of infinite plane wave beams, phase matching gives an infinite interaction length. In practice beams are finite in extent, and other factors such as double refraction [4]–[7] and diffraction [6]–[8] serve to limit the interaction length. The first phase-matching experiments [2], [3] were not able to elucidate these factors. There, the interaction length was limited [6] to the ~ 1 mm coherence length of the pulsed ruby laser. It was not until the introduction of the gas laser technique [9]–[11] for studying SHG that the true limitations on interaction length under phase-matched conditions could be studied experimentally in detail.

Manuscript received December 23, 1965.

The authors are with the Bell Telephone Laboratories, Inc., Murray Hill, N. J.

It was found that the gas laser, because of its single transverse mode [12], [13] capability, could produce considerable SHG power on a CW basis, in spite of its relatively low power. Working in the lowest-order transverse mode of a 3.4 mm diameter beam close to the beam minimum permitted observation of interaction over the full length of a 1.2 cm-long KDP crystal, and led to a new determination of the nonlinear coefficient [9] of KDP. Further work [7], [8] on crystals as long as 5 cm and 10 cm showed, both experimentally and theoretically, how double refraction limits the interaction length in essentially parallel beams of finite transverse extent. Due to the physical separation of the ordinary wave fundamental beam from the second harmonic extraordinary wave beam, efficient interaction can be maintained up to a length l_a , called the aperture length [7], where

$$\frac{l_a}{w_0} = \frac{\sqrt{\pi}}{\rho} \quad (1)$$

w_0 is the fundamental beam radius at which the electric field amplitude is down to $1/e$ of its axial value, and ρ is the double-refraction angle between ordinary and extraordinary wave Poynting vectors.

The harmonic power in the phase-matched direction for a plane parallel beam when the effects of double refraction and diffraction are neglected can be written [7] as

$$P_2 = KP_1^2 l^2 / w_0^2 \quad (2)$$

where

$$K = \frac{128\pi^2 \omega_1^2}{(n_1 c)^3} d_{36}^2 \sin^2 \theta_m \quad (3)$$

and ω_1 is the fundamental frequency, n_1 the index of refraction, d_{36} the nonlinear coefficient [9], and θ_m the phase-matching angle as measured from the optic axis. In KDP at 1.1526μ for the fundamental, $K = 1.52 \times 10^{-16}$ esu. In the region of full interaction up to $l \sim l_a$, the harmonic power P_2 grows as l^2 . Beyond l_a , the power grows linearly as l/w_0^2 . Thus, double refraction limits the rapid growth of harmonic output for crystals of finite ρ in the near field with essentially parallel beams.

Diffraction effects become predominant if the interaction extends into the far field. The effects of diffraction have been studied both theoretically and experimentally by KAB [8] in an investigation of SHG from focused laser beams. They show that, in a crystal of infinite length, the SHG from a focused fundamental beam,

including double refraction and diffraction, is given by

$$P_2 = KP_1^2 \frac{l_f l_a}{w_0^2} \quad (4)$$

providing $l_a \ll l_f$;

$$l_f = \frac{\pi}{2} b \quad (5)$$

is defined as the effective length of a focused beam; b is the confocal parameter of the fundamental beam [12], [13]. It is related to the beam radius by

$$w_0^2 k_1 = b \quad (6)$$

where $k_1 = n_1 \omega_1 / c$ is the propagation constant of the fundamental in the medium of index n_1 . The length b is the distance between the two points along the beam at which the beam radius has increased by a factor of $\sqrt{2}$ over its value at the beam waist.

If ρ can be made zero, as in the case of LiNbO₃ [14], [15], the aperture length becomes infinite. For this case, and also when $l_a \gg l_f$, KAB show that the total SHG is given by

$$P_2 = KP_1^2 \frac{4l_f^2}{w_0^2} \quad (7)$$

Thus, for focused beams where the interaction extends to the far field, it can be said, as a good approximation, that the effective interaction falls off beyond a length equal to l_f .

We shall see that, for any situation where the interaction length is limited by l_a or l_f , optical feedback or resonance can be used effectively to extend the interaction length and enhance the amount of harmonic conversion. Qualitatively, the idea is that, when the output harmonic beam begins to grow at less than the maximum l^2 rate, it is reflected back and refocused by an optical resonator in such a phase that it can continue to interact with the fundamental power. In this way the effective length of interaction can be increased greatly. Resonance of the harmonic radiation to increase harmonic output has been mentioned previously [4], [16]–[18]. Also of relevance here is the possibility of resonating the incident fundamental beam [4], [17]–[20]. This is simply a means of storing the incident energy in a high Q cavity to increase the flux of fundamental power passing through the crystal, thereby increasing the generation of second harmonic power. An alternative approach to these resonant enhancement schemes is to use optical waveguide techniques [21] to increase the interaction length.

Aside from the question of increased harmonic output, another motivation for this study of resonance effects lies in the application of nonlinear optics to parametric processes. As is well known [4], [22]–[25], parametric gain is possible in nonlinear difference mixing. Both the signal wave and the wave at the difference frequency (idler wave) extract energy from the pump wave and are amplified. This amplification, even if modest, can be utilized to make a parametric oscillator,

if use is made of a high Q optical resonator to give feedback. Thus, resonant SHG, mixing, and parametric oscillators are closely related.

In Section IV it is shown how the realities of optical loss, mechanical instabilities, optical feedback, and resonator lineup are dealt with. The experimental results clearly show large resonant enhancements which are in good agreement with theory. Because of the high optical Q achieved with harmonic resonance, it is possible to show in graphic form the detailed response to the longitudinal mode spectrum of the laser. In addition to harmonics of the individual modes, the sums of all pairs of modes are also shown.

The experimental part of this study is a natural extension of the previously reported gas laser experiments [7], [9]. For resonance work, the high degree of mode control and the continuous output are particularly required for careful measurements.

The analysis presented in Sections II and III extends existing theory [7], [8] to handle resonant nonlinear effects due to single transverse mode laser beams. The equilibrium resonator fields are deduced on the basis of a self-consistent field approach which has the advantage of easy physical understanding. The detailed transverse field distributions are used to determine a mode-coupling factor [26] which gives the coupling of the generated light to the Gaussian resonator modes. Expressions for the resonant half-widths and the enhancement factors are put in terms of resonator losses and coupling factors in a form which permits direct experimental comparison. The factors governing the choice of the resonator geometry are studied in detail.

II. RESONANCE OF THE SECOND HARMONIC

In this section we discuss the theoretical effect of resonating the second harmonic radiation generated in the nonlinear medium. Figure 1 shows schematically the geometry of the harmonic resonance technique. The fundamental power is assumed to make only a single pass through the crystal. Mirror M_1 and M_2 are assumed to be highly reflecting for the harmonic, and aligned so as to reflect the generated harmonic back to the input, where it can interact again in the nonlinear crystal. One of the mirrors (M_2) is made movable, so that the mirror separation, and therefore the phase of the reflected harmonic field, can be varied. The system constitutes a tunable resonator. As the resonator is tuned through the harmonic frequency, the harmonic power generated shows a strongly resonant response. Physically, one expects enhancement of the generated power in such a resonator, since the presence of harmonic electric field enhances the power radiated from the harmonic polarization. The fact that harmonic power grows as the square of the crystal length in the phase-matched direction is the simplest illustration of this point. In Section II-A we relate the resonant response to the resonator losses, and compute the enhancement factor which gives the ratio of the harmonic power at the peak of the reso-

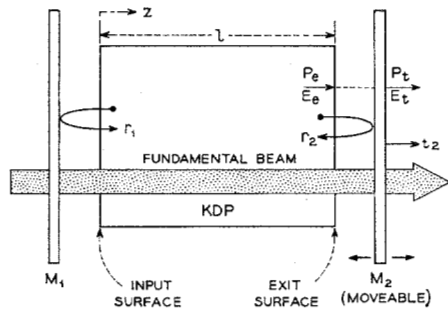


Fig. 1. Schematic of the geometry of the harmonic resonance technique as applied to a KDP nonlinear crystal. Mirrors M_1 and M_2 are transparent to the fundamental and highly reflecting to the harmonic.

nance to the power generated in a single pass through the crystal. In Section II-B we compute the ratio of the change in mirror separation between successive harmonic resonances ($\lambda_2/2$) to the change in mirror separation between half-power points of the resonance (δ). This ratio is observed directly in the experiment and provides a convenient point of comparison with the theory. Section II-C considers the coupling of the harmonic transverse field distribution to the modes of the harmonic resonator.

The transverse field distribution of SHG radiation is not the same as that of the fundamental, due to the effects of double refraction, as was first pointed out by Kleinman [6] and ABDP [4]. Recently, BADK [7] have elaborated on this in detail for a parallel beam, and KAB [8] for a focused beam. They find the exact shape of the asymmetric harmonic beam generated by an incident Gaussian fundamental beam. BADK [7] define an aperture length l_a as in (1). When $l \ll l_a$, double refraction is negligible. The transverse field distribution of the harmonic is the closely Gaussian, with a radius $1/\sqrt{2}$ times that of the fundamental. For $l \sim l_a$ or greater, the transverse field becomes increasingly asymmetric. In the manner of Kogelnik [26], we find the coupling coefficient which gives the fraction of the asymmetric power that couples to the lowest-order Gaussian mode (TEM_{00}) and the next higher-order Gaussian mode (TEM_{10}) of the resonator. This is done by expanding the field in terms of the complete set of eigenfunctions or modes of the resonator via a Fourier integral expansion. The result is given as a function of l/l_a . The coupling coefficient is included in Sections II-A and II-B as a parameter, and is finally evaluated in Section II-C.

A. Theory of Resonance Effects

We restrict our discussion here to the near-field case, where diffraction is negligible. We start by briefly reviewing some of the results of BADK [7] for the single-pass harmonic generation in the absence of any resonant feedback. Assume that the fundamental beam travels in the z direction of a Cartesian coordinate system xyz , and that the crystal optic axis lies in the xz plane. BADK [7] show that the increment in harmonic electric field E_2 in the phase-matched direction is proportional to the

fundamental intensity $S_1(x, y)$

$$\frac{dE_2}{dz} = iJS_1. \quad (8)$$

The imaginary i arises from the use of complex notation. In (8) it serves to indicate that the harmonic field is 90° out of phase with the harmonic polarization wave. J is a constant containing the nonlinear coefficient. The harmonic electric field at the exit surface $z = l$ of the crystal may be written as in [7], eq. 3.22

$$E_2(x, y) = iJS_0 l F(u, t, q) e^{-\alpha_1 l/2} e^{-\alpha_2} \quad (9)$$

where S_0 is the peak of the fundamental Gaussian intensity described by

$$S_1(x, y) = S_0 e^{-2(x^2+y^2)/w_0^2}. \quad (10)$$

The function F used in (9) describes the transverse x variation of the harmonic electric field at the exit surface.

$$F(u, t, q) = \frac{1}{t} \int_0^t e^{-2a\tau} e^{-(u+\tau)^2} d\tau, \quad (11)$$

u and v are normalized transverse coordinate variables given by

$$\begin{aligned} v &= y/w_2 \\ u &= \frac{\sqrt{2} x_2}{w_0} \end{aligned} \quad (12)$$

where x_2 is the transverse coordinate in the x direction measured from the ρ line, as defined in BADK [7], eq. 3.18. The harmonic beam radius w_2 is related to the fundamental beam radius w_0 by

$$w_2 = \frac{w_0}{\sqrt{2}}. \quad (13)$$

Also, t is a normalized length,

$$t = \sqrt{2\pi} \frac{l}{l_a} \quad (14)$$

and the quantity

$$q = \frac{\alpha w_0}{2\sqrt{2} \rho} \quad (15)$$

where

$$\alpha = \alpha_1 - \frac{\alpha_2}{2} \quad (16)$$

is a normalized loss parameter. The transverse field variation of the extraordinary wave harmonic (9) at the exit surface is shown in Fig. 2 by the curve labeled E_2^* (single pass) for the case of no loss. For reference, the incident Gaussian ordinary wave fundamental field is shown labeled $E_1^0(TEM_{00})$. The other aspects of Fig. 2 will be discussed later. The resulting SHG power in a crystal of length l with no resonance effects may be written (BADK [7], eq. 3.32).

$$P_2 = KP_1^2 \frac{l^2}{w_0^2} e^{-\alpha_1 l} G \quad (17)$$

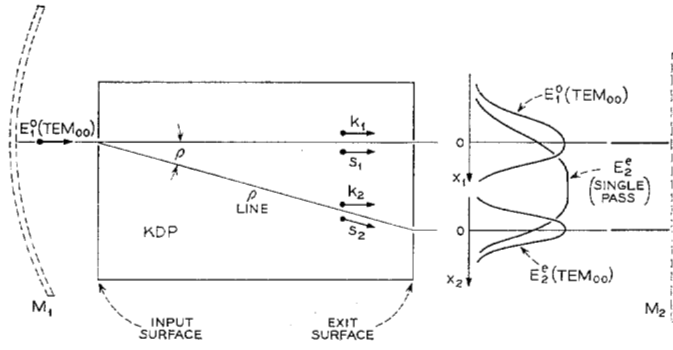


Fig. 2. Sketch showing the propagation of the fundamental and harmonic beams in KDP, and the shape of the electric field distributions at the exit surface for the case of no loss.

where

$$G(t, q) = \left(\frac{2}{\pi}\right)^{1/2} \int_{-\infty}^{+\infty} F^2(u, t, q) du. \quad (18)$$

The function G represents the reduction in SHG power due to double refraction from that given by one-dimensional considerations alone. In the limit of $\rho \rightarrow 0$ ($l \ll l_a$) and no loss, $G = 1$ and (17) is identical to that given by (2).

To treat the case of resonance of the harmonic, let us refer again to Fig. 1 and define E_e as the complex harmonic electric field existing in the resonator at the exit surface just inside the crystal. Let r_2 be the power reflection coefficient at the right side of the crystal, as seen from inside the crystal. This coefficient will thus include surface reflection losses as well as external mirror losses. Define the power transmission coefficient t_2 , relating the transmitted electric field E_t to the resonator electric field E_e , as follows

$$E_t = \sqrt{nt_2} E_e \quad (19)$$

where n is the index of refraction of the harmonic in the crystal (since E_e is defined as the field inside the crystal). Conservation of energy requires

$$r_2 + a_2 + t_2 = 1 \quad (20)$$

where a_2 is the power-loss coefficient which includes all of the losses in the dielectric mirror, plus the losses at the surface of the crystal, assuming that this power is scattered from the resonator. In the experimental situation, the surface losses are low, being comparable with mirror losses. Also define r_1 as the power-reflection coefficient at the left surface of the crystal, as viewed from within the nonlinear medium.

Since the fundamental beam travels only from left to right, no second harmonic power is generated as the harmonic wave travels from right to left after reflection from the right-hand mirror. The complex SHG field intensity E_e in the lowest transverse mode of the harmonic resonator is given by the self-consistency equation

$$E_e = re^{i\varphi} E_e + c_{a0} E_2 \quad (21)$$

where the single-pass harmonic electric field at the exit

surface E_2 was defined in (9); r is defined by

$$r = \sqrt{r_1 r_2} e^{-\alpha_2 l}, \quad (22)$$

φ is the round-trip phase shift within the resonator. The single-pass absorption of the harmonic electric field is $e^{-\alpha_2 l/2}$.

Thus, $(1 - r^2)$ is the round-trip power absorption; c_{a0} is the electric field coupling coefficient between the transverse field distribution of the SHG and the lowest-order transverse mode of the harmonic resonator (c_{a0} will be evaluated later). From (21) one obtains

$$E_e = \frac{c_{a0} E_2}{1 - re^{i\varphi}}. \quad (23)$$

The total unidirectional SHG power inside the resonator is obtained from $E_e \cdot E_e^*$ as

$$P_e = \frac{\kappa P_2}{(1 - 2r \cos \varphi + r^2)} \quad (24)$$

where the power coupling coefficient is

$$\kappa = c_{a0}^2. \quad (25)$$

The harmonic power transmitted through the mirror on the right is given by

$$P_t = t_2 P_e = \frac{\kappa t_2 P_2}{(1 - r)^2 + 4r \sin^2 \frac{\varphi}{2}}. \quad (26)$$

At resonance, where $\varphi = 0$, the resonant enhancement factor for the transmitted harmonic power is

$$\frac{P_t}{P_2} = \frac{\kappa t_2}{(1 - r)^2}. \quad (27)$$

This can be quite large. For example, if $a_2 = \alpha_2 = 0$ and $r_1 = r_2 = 0.99$, the transmitted power is enhanced by a factor of 100κ over that which would occur without resonance. Inside the resonator, the harmonic power is enhanced by $10^4 \kappa$. The value of κ is typically between ~ 0.3 and unity.

Derivations similar to the one given in (21)–(27) for the lowest-order transverse mode also apply for each of the higher-order modes, if we simply interpret κ , φ , and r as applying to the appropriate mode under consideration. In general, we expect r to be independent of mode number; κ and φ , in general, vary with mode number. More will be said about these later.

B. Width of Harmonic Resonance and Resonator Q

The width of the harmonic resonance relative to the spacing between successive resonance is derived from (26) by considering the variation of P_t for small departures from resonance; that is, for $\varphi \ll 1$. Define

$$\epsilon = 1 - r \quad (28)$$

as the average one-way harmonic power loss within the resonator. The phase shift within the resonator between

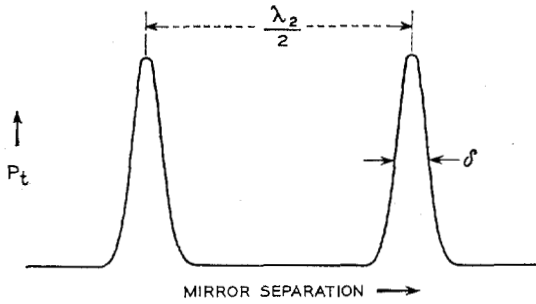


Fig. 3. Expected resonant behavior of the harmonic power as the mirror separation of the harmonic resonator is varied.

half-power points is

$$2\phi_h = \frac{2(1-r)}{\sqrt{r}} \approx 2\epsilon \quad (29)$$

for $\epsilon \ll 1$.

To produce a change in the round-trip phase change of $2\phi_h$ between half-power points of the resonance, we must change the mirror separation by an amount $\Delta z = \delta$ in free space, where

$$2\phi_h = 2k_2\delta = 2\epsilon. \quad (30)$$

One can shift the longitudinal mode number by unity by a change in the round-trip phase shift of 2π , corresponding to a change in mirror separation $\Delta z = \lambda_2/2$ in free space.

Consequently,

$$\frac{2\pi}{2\phi_h} = \frac{\lambda_2/2}{\delta} = \frac{\pi}{\epsilon} \quad (31)$$

gives the ratio of the spacing of the longitudinal resonances to the width before half-power points, as illustrated in Fig. 3.

For comparison, consider the resonant response of a conventional passive resonator fed by a fixed frequency source as the mirror separation is varied. From *BG* [12], the Q of a resonator is given by

$$Q = \frac{\text{stored energy}}{\text{energy loss per second}} = \frac{2\pi d}{\epsilon\lambda} \quad (32)$$

where d is the effective optical length of the resonator, λ is the wavelength, and ϵ is the one-way loss per pass, including one reflection. As the frequency of the resonator is swept by varying the length d , the distance δ between half-power points is clearly

$$Q = \frac{f}{\Delta f} = \frac{d}{\delta} \quad (33)$$

From (32) and (33), one obtains

$$\frac{\lambda/2}{\delta} = \frac{\pi}{\epsilon} \quad (34)$$

which is the same as (31) for harmonic resonance. This is, perhaps, obvious. It says that the loss alone determines the resonant response, and not the strength of the non-linear interaction driving the resonator.

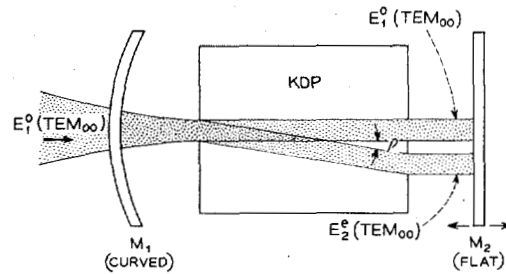


Fig. 4. Plano-concave resonator and the relative location of the ordinary fundamental beam $E_1^o(TEM_{00})$ and the extraordinary harmonic beam $E_2^e(TEM_{00})$.

C. Coupling Coefficient as a Function of l/l_a

Figure 2 sketches the geometry and electric field distributions at the exit surface of the crystal needed for the calculation of the coupling coefficient. The curved mirror M_1 and the plane mirror M_2 , shown dotted in Fig. 2, are highly reflecting to the harmonic, but transmitting for the fundamental, and constitute a plano-concave harmonic resonator, as shown in Fig. 4. The details of the choice of this resonator are discussed in Section IV-A. The incident ordinary wave fundamental field which drives the crystal is a TEM_{00} Gaussian mode field, shown in Fig. 2 as $E_1^o(TEM_{00})$ at the exit surface. The curve labeled E_2^e (single pass) represents the single-pass extraordinary wave harmonic field generated by a single pass of $E_1^o(TEM_{00})$ through the crystal in a non-resonant interaction. As we see, the harmonic is no longer Gaussian and emerges asymmetrically with respect to the fundamental, due to double refraction. The field E_2^e (single pass) drives the various modes of the harmonic resonator. In particular, we calculate the coupling to the lowest-order extraordinary wave field of the harmonic resonator, shown in Fig. 2 as the Gaussian [labeled $E_2^e(TEM_{00})$] and the next higher-order extraordinary wave field $E_2^e(TEM_{10})$. Both of these modes are centered around the ρ line at the exit surface.

The coupling coefficient to these modes of the harmonic resonator will be found with two major assumptions. First, that there is no loss [i.e., $\alpha_1 = \alpha_2 = q = 0$ in (12) and (16)], and, second, that the crystal is in the near field of the resonator mode, so that diffraction effects can be neglected. Both of these assumptions are valid for the resonator used, as will be seen in Section IV. We normalize the field $E_2^e(TEM_{00})$ and E_2^e (single pass) to unit power, and then compute the coupling. The $E_2^e(TEM_{00})$ eigenfunction can be expressed in terms of the transverse coordinate x_2 measured from the ρ line,

$$\psi_{00}(x, y) = \psi_0(x)\psi_0(y) = \frac{2}{w_0\sqrt{\pi}} e^{-2(x_2^2+y^2)/w_0^2} \quad (35)$$

where we have replaced the beam radius of the harmonic w_2 in the usual field expression by $w_0/\sqrt{2}$ from (11). Note that

$$\iint_{-\infty}^{+\infty} \psi_{00}^2 dx dy = 1. \quad (36)$$

From Section 3.1 of BADK [7], we write the transverse electric field distribution E_z^s (single pass) as

$$f(x)g(y) = \frac{2}{w_0 \sqrt{\pi} \sqrt{G}} F \cdot e^{-2y^2/w_0^2} \quad (37)$$

where F and G are given in (11) and (18), with $q = 0$. Using (13) and (18), one can verify that

$$\iint_{-\infty}^{+\infty} f^2(x)g^2(y) dx dy = 1. \quad (38)$$

Define, following Kogelnik [26], the electric field coupling coefficient due to the aperture length to the lowest transverse mode as

$$\begin{aligned} c_{a0} &= \iint_{-\infty}^{+\infty} f(x)g(y)\psi_{00}(x, y) dx dy \\ &= \int_{-\infty}^{+\infty} f(x)\psi_0(x) dx_2. \end{aligned} \quad (39)$$

Substituting from (12) for F , and interchanging the order of integration, one obtains successively

$$\begin{aligned} c_{a0} &= \frac{2}{w_0 \sqrt{\pi G}} \int_{-\infty}^{+\infty} F \cdot e^{-2x_2^2/w_0^2} dx \\ &= \sqrt{\frac{2}{\pi G}} \int_{-\infty}^{+\infty} F(u, t)e^{-u^2} du \\ &= \frac{1}{t\sqrt{G}} \int_0^t e^{-\tau^2/2} d\tau. \end{aligned} \quad (40)$$

Thus

$$c_{a0}(t) = \frac{1}{t\sqrt{G(t, 0)}} \sqrt{\frac{\pi}{2}} \operatorname{erf}(t/\sqrt{2}). \quad (41)$$

In the limiting case of $t \ll 1$, where t is defined by (14), note that

$$c_{a0} = \frac{1}{\sqrt{G}} \rightarrow 1. \quad (42)$$

The power-coupling coefficient is given by (25). Using the evaluation of $G(t, 0)$ from BADK [7], eq. 3.38, with (41) and (25), we obtain the curve of $c_{a0}^2(t)$ shown in Fig. 5. When $l = l_a$, $c_{a0}^2 = 0.35$, and the coupling to the TEM_{00} mode of the resonator is 35 percent. In the limiting case of large l/l_a ($t \gg 1$)

$$c_{a0}^2(t) = \frac{1}{2t} \sqrt{\frac{\pi}{2}} \ll 1. \quad (43)$$

From (14) and (17) and BADK [7], eq. 3.39, one observes that for $t \gg 1$

$$c_{a0}^2 P_2 = KP_1^2 \frac{l_a^2}{4w_0^2} \quad (44)$$

which is independent of l , showing that resonant harmonic generation in this mode has ceased to increase with crystal length.

In a similar fashion, one may evaluate the coupling to

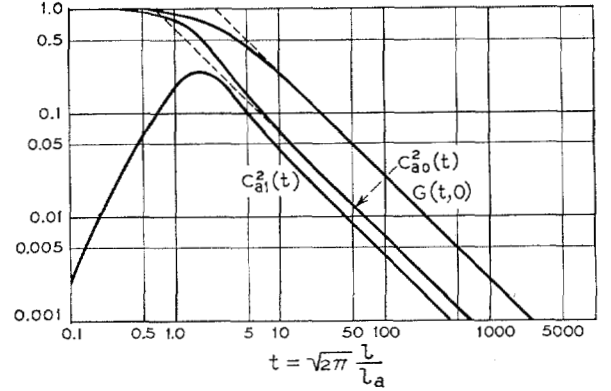


Fig. 5. Variation of the power coupling coefficient to the TEM_{00} mode and TEM_{10} mode of the harmonic resonator, labeled c_{a0}^2 and c_{a1}^2 , respectively, as a function of the dimensionless length parameter t .

the TEM_{10} mode

$$c_{a1} = \int_{-\infty}^{+\infty} f(x)\psi_1(x) dx_2 \quad (45)$$

where

$$\psi_1(x) = \frac{4x_2}{\pi^{1/4} w_0^{3/2}} e^{-2x_2^2/w_0^2}. \quad (46)$$

One then obtains

$$c_{a1}(t) = \frac{-(1 - e^{-t^2/2})^2}{t\sqrt{G(t)}}. \quad (47)$$

The limiting cases for the power-coupling coefficient for this mode is, from (25), given by

$$\begin{aligned} c_{a1}^2(t) &\rightarrow \frac{t^2}{4} & t \ll 1 \\ &\rightarrow \frac{1}{\sqrt{2\pi} t} & t \gg 1 \end{aligned} \quad (48)$$

and

$$\frac{c_{a1}^2}{c_{a0}^2} \rightarrow \frac{2}{\pi} \quad t \gg 1. \quad (49)$$

$c_{a1}^2(t)$ is plotted in Fig. 5, where it is seen that the coupling to the TEM_{10} mode decreases rapidly for small t , as is reasonable. The couplings to the other higher-order modes were not explicitly calculated, although we expect them to decrease steadily with increasing order.

From Fig. 5, we see in the limit $t \ll 1$ that $c_{a0}^2(t) \rightarrow 1$ and $c_{a1}^2(t) \rightarrow 0$, as do all the higher-order couplings. For a crystal like KDP with finite ρ and therefore finite l_a , small t implies a short crystal length l . However, for LiNbO_3 , where phase-matched operation normal to the optic axis is possible, $\rho = 0$ and $l_a = \infty$ [14], [15]. Thus, for such crystals of any reasonable length l , we are still in the $t \ll 1$ limit, where there is 100 percent coupling to the lowest-order Gaussian mode of the harmonic resonator. This result, although derived for the near field only, applies more generally to the far field, and implies that both fundamental and harmonic are TEM_{00} modes which

diffract together into the far field with coincident phase fronts. Thus, harmonic resonance with LiNbO_3 should be quite favorable.

III. RESONANCE OF THE FUNDAMENTAL

Assume we have a fundamental resonator with mirrors M_1 and M_2 which are highly reflecting at the fundamental wavelength and perfectly transmitting at the harmonic wavelength, as shown in Fig. 6. If the resonator is properly matched, then, at resonance, the fundamental power passing through the crystal inside the resonator is greater than the single-pass power through the crystal in the absence of the mirrors. Since SHG power is proportional to the square of the fundamental power, enhanced SHG is possible, using the fundamental resonator.

The power inside the resonator and the matching condition can be derived, following the approach of Section II-A. Rack and Biazzo [27] have derived similar results from a different approach. Referring to Fig. 6, define r_1 and r_2 as the power-reflection coefficients, and t_1 and t_2 as the transmission coefficients at the lossless mirrors M_1 and M_2 . Let t be the fundamental power-transmission coefficient of the crystal. r_1 , r_2 and t are all close to unity. By definition

$$r_1 + t_1 = 1 = r_2 + t_2. \quad (50)$$

Define P_1 , P_r , and P_c , respectively, as the incident power, reflected power, and the power inside the mirror M_1 of the resonator incident on the crystal. We express these powers in terms of the round-trip phase shift within the resonator φ and a reflectance parameter defined as

$$r_m = t^2 r_2. \quad (51)$$

We find

$$\frac{P_c}{P_1} = \frac{t_1}{(1 - \sqrt{r_1 r_m})^2 + 4\sqrt{r_1 r_m} \sin^2 \frac{\varphi}{2}} \quad (52)$$

$$\frac{P_r}{P_1} = \frac{(\sqrt{r_1} - \sqrt{r_m})^2 + 4\sqrt{r_1 r_m} \sin^2 \frac{\varphi}{2}}{(1 - \sqrt{r_1 r_m})^2 + 4\sqrt{r_1 r_m} \sin^2 \frac{\varphi}{2}}. \quad (53)$$

The power transmitted through the resonator is equal to $t_2 P_c$, where P_c is given in (52). At resonance, $\sin^2 \varphi/2 = 0$, and the reflected power is given by

$$\frac{P_r}{P_1} = \frac{(\sqrt{r_1} - \sqrt{r_m})^2}{(1 - \sqrt{r_1 r_m})^2}. \quad (54)$$

If the input mirror reflectivity $r_1 = r_m$, the reflected power $P_r = 0$, and the resonator is matched. This match condition implies that the coupling loss $1 - r_1$ is equal to the sum of all other losses $1 - t^2 r_2$, as for microwave and other resonators. Let P_{cm} be the power in the cavity at mirror M_1 when we are matched and at resonance;

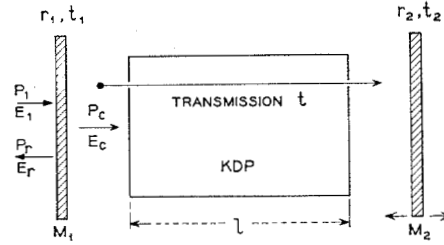


Fig. 6. Fundamental resonator with mirrors M_1 and M_2 , which are highly reflecting to fundamental light and transmitting to harmonic light.

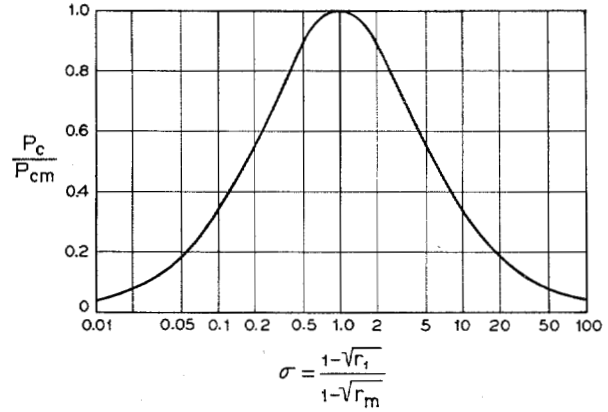


Fig. 7. Variation of the normalized power inside the fundamental resonator with the mismatch parameter σ .

that is, $r_1 = r_m$ and $\sin^2 \varphi/2 = 0$. Then

$$\frac{P_{cm}}{P_1} = \frac{1}{1 - r_m}. \quad (55)$$

The square of (55), that is, $1/(1 - r_m)^2$, gives the resonant enhancement of SHG due to fundamental resonance.

We now find the sensitivity of P_c to departures of r_1 from the ideal matching situation. From (52), (50), and (55), at resonance,

$$\frac{P_c}{P_{cm}} = \frac{(1 - r_1)(1 - r_m)}{(1 - \sqrt{r_1 r_m})^2} = \frac{2(1 + \sqrt{r_m})\sigma - (1 - r_m)\sigma^2}{(\sigma\sqrt{r_m} + 1)^2} \quad (56)$$

where

$$\sigma = \frac{1 - \sqrt{r_1}}{1 - \sqrt{r_m}} > 0. \quad (57)$$

If $(1 - r_1) \ll 1$ and $(1 - r_m) \ll 1$, then $\sigma \approx (1 - r_1)/(1 - r_m)$, and

$$\frac{P_c}{P_{cm}} \approx \frac{4\sigma}{(\sigma + 1)^2}. \quad (58)$$

This is plotted in Fig. 7. From the fact that the curve is symmetrical about $\sigma = 1$ on a log plot, we conclude that, for a given deviation from match, it is better to be over-coupled ($\sigma > 1$) than under-coupled ($\sigma < 1$). Note that significant deviations from match still give considerable enhancement of the fundamental power P_1 within the resonator.

IV. DESCRIPTION OF THE EXPERIMENT

The experimental setup selected for this study consisted of a fixed-frequency gas laser and a separate tunable external resonator containing the nonlinear crystal. By separating the laser resonator from the external resonator, one achieves the greatest flexibility in the choice of parameters for each of the resonators. Furthermore, if one can succeed in optically isolating the source from the tunable resonator, one is then able to measure and interpret separately the characteristics of the laser source and the harmonic output of the external resonator. These features are highly desirable in an experimental study. Under different circumstances, however, it might be desirable to work internally to the laser cavity, to take advantage of the high internal energy flux.

A. Resonator Considerations

1) *Harmonic Resonator*: The harmonic resonator used is shown schematically in Fig. 4. The 1-meter curved mirror M_1 and the flat mirror M_2 were separated by 3 cm and were highly reflecting for the harmonic and highly transmitting for the fundamental. The actual sample used for the resonance work consisted of a 1.23 cm length of KDP, with a pair of 1 mm thick antireflection-coated fused quartz plates optically joined to the KDP with index matching fluid. This type resonator is inherently high Q and relatively insensitive to small angular misadjustments. Quantitative experimental comparisons with other resonator geometries, as discussed in Section V, bear out these statements. Table I contains a summary of various harmonic resonator and sample parameters used.

TABLE I

b	w_2	δ_2	ξ_{KDP}	l_a	l/l_a
31.4 cm	0.017 cm	1.08×10^{-3}	0.030	1.4 cm	0.87

In arriving at the results of Table I, correct account must be taken of the presence of the 1.43 cm of dielectric in the resonator. The problem of an optical resonator partially filled with dielectric is of importance in practice, and has not been treated in the literature. What is required is to find the equivalent length of the air-dielectric combination in a problem involving the diffractive spread of a beam. Kogelnik [28] has described the ray matrix, or $ABCD$ method, for relating the transverse position and slope of a ray at the input and output reference planes of an optical system. This can be applied to resonators where we can specify the characteristics of the resonator by relating the position and slope at one mirror to the same quantities at the other mirror. Looking at Fig. 4, we see that the region between mirrors can be divided into three optical regions by imagining two additional reference planes placed in air adjacent to the dielectric material of length l and index n . For the

dielectric region, the matrix is easily shown to be [82]

$$\begin{Bmatrix} x_0 \\ x'_0 \end{Bmatrix} = \begin{Bmatrix} 1 & l/n \\ 0 & 1 \end{Bmatrix} \begin{Bmatrix} x_i \\ x'_i \end{Bmatrix}. \quad (59)$$

To get the matrix for the other two regions containing only air, let $n = 1$. The product of these three matrices is then the matrix-relating positions and slopes of rays at the two reference planes at the mirror

$$\begin{Bmatrix} 1 & l_s + (l/n) \\ 0 & 1 \end{Bmatrix} \quad (60)$$

where l_s is the total air length within the resonator on both sides of the crystal. The matrix (60) indicates that the equivalent air length of the resonator is

$$d_s = l_s + \frac{l}{n} \quad (61)$$

irrespective of the location of the crystal within the resonator. For the plano-concave resonator, the equivalent confocal parameter b is [12],

$$b^2 = 4db_1 - 4d^2 \quad (62)$$

where b_1 is the curvature of mirror M_1 and d is the length of the resonator in air (vacuum). Using $b_1 = 1$ m, $l_s = 1.6$ cm, $l = 1.4$ cm, $n = 1.5$, and $d = d_s = 2.53$ cm, we get $b = 31.4$ cm, as shown in Table I, using (61) and (62).

It is important to note that there is a second equivalent length which applies to the calculation of the axial mode spacing or free spectral range of a resonator. For a resonator containing only air (vacuum), this is $c/2d$, where d is the resonator length. For a resonator partially filled with an antireflection-coated dielectric, $d = d'_s$ where

$$d'_s = l_s + nl \quad (63)$$

since the actual number of wavelengths in the dielectric is increased by the index of refraction n .

The beam radius w_2 of the harmonic at the plane mirror of the plano-concave resonator is found from (5), using b and the free-space propagation constant. The far-field diffraction angle [7], [12] is given by

$$\delta_0 = \frac{2w_0}{b} \quad (64)$$

and is listed as δ_2 in Table I for the harmonic resonator. The parameter [12]

$$\xi = \frac{l}{b} \quad (65)$$

is a normalized distance that determines the diffractive spread of the beam, according to

$$w^2 = w_0^2(1 + \xi^2) \quad (66)$$

where w_0 is the beam radius at the beam minimum, and w is the radius at distance ξ away. If $\xi \ll 1$, beam spread or diffraction is small, and one is in the near field. Thus, $\xi_{KDP} \approx d/b \approx 0.030$ gives the diffractive spread in the KDP crystal, and is small. The aperture length l_a is

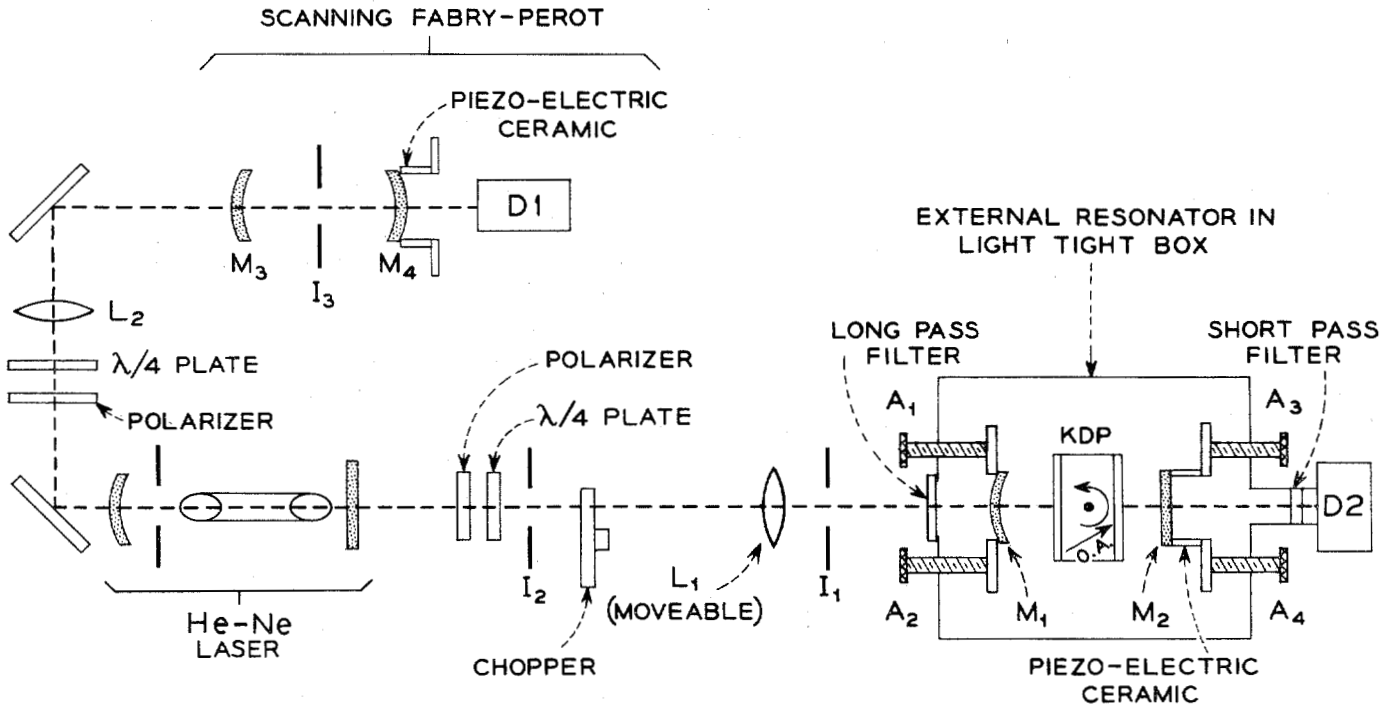


Fig. 8. Sketch of the experimental setup.

defined in (1). The quantity l/l_a gives the ratio of the sample length to the aperture length.

2) *Fundamental Resonator*: The plano-concave resonator of Fig. 4 could be used for studying resonance of the fundamental, if mirrors M_1 and M_2 were made highly reflecting at the fundamental and highly transmitting at the harmonic. Only a limited amount of work was, in fact, done in resonance of the fundamental and, for this, a plane-parallel resonator was used.

3) *Resonator for Simultaneous Harmonic and Fundamental Resonance*: Simultaneous resonance of fundamental and harmonic frequencies is an attractive thought. However, as mentioned by Kingston and McWhorter [18], if the standing wave nulls of the electric field of the fundamental and harmonic coincide as at a common conductive mirror, the interaction between harmonic and fundamental becomes zero because of the equal and opposite effect of waves traveling in both directions within the resonator. They [18] point out that this may be overcome experimentally by separate mirror surfaces for fundamental and harmonic, or possibly by operating with some phase mismatch.

This will not be pursued further here, since no experiments were attempted.

B. Experimental Setup

Figure 8 shows a sketch of the experimental setup, showing the laser source, external resonator, with its KDP sample clad in antireflection-coated quartz plates, and all other relevant components. The external resonator consisted of a pair of dielectrically coated mirrors which could be adjusted in angle and whose separation could be varied by piezoelectrically scanning one of them. A sample holder located the nonlinear crystal with the

optic axis, as shown between the mirrors, with adjustments on its angle and position. By changing mirrors in the external resonator, it was possible to study resonance of the harmonic and of the fundamental separately. The use of the scanning technique not only permits one to obtain directly the complete resonant response of the harmonics from the external resonator, but also avoids what would otherwise be the difficult problem of setting on the peak of the optical resonance.

The resonator, including detector, was located inside a light-tight box with adjustments emerging through flexible joints. A long wavelength pass filter on the input end of the box excluded visible light and passed the fundamental beam at 1.15μ . The detector, which was a 6199 photomultiplier or, occasionally, a 1P21, was shielded from the 1.15μ radiation and exposed to the 0.576μ harmonic radiation by a short wavelength pass filter. The output of the photomultiplier was processed by a phase-sensitive detection circuit having a suitable time constant and displayed on a chart recorder driven in synchronism with the piezoelectric mirror drive.

The scanning Fabry-Perot spectrometer [29] set up on the back end of the laser measured the amplitudes and spacings of the longitudinal modes of the 1.15μ laser used to drive the external resonator. It also could detect coupling of the external resonator at resonance to the laser. Coupling causes a considerable increase in the jitter of the amplitudes and spacings of the modes. In the harmonic resonator experiments, the coupling was due to residual mirror reflections at the fundamental frequency. A polarizer and quarter-wave plate-type isolator was not used in the final measurements, since it introduced loss and operated with degraded isolation, due to differences in the reflection coefficient

of the resonator for ordinary and extraordinary polarizations. It was found that the coupling could be reduced to tolerable levels by using a very high-reflectivity mirror as output mirror in the laser.

Coupling was more noticeable when resonating the fundamental. However, for our experiment, it was not bothersome, due to the low Q of the plane-parallel resonator used, as will be discussed later. In principle, if the reflectivity of the input mirror $r_1 = r_m$, as given in (51), then the resonator is matched and there is no reflected power. In practice a special mirror of continuously variable reflectivity was slid across the beam to adjust for best match. This mirror had tapered dielectric layers which caused the reflectivity to vary with position across the mirror. Over one inch of travel, the reflectivity changed continuously from ~ 96 percent to ~ 30 percent. This, unfortunately, was so rapid a change that variations over the beam diameter were significant. For this reason, and partly for reasons associated with the low Q , it was not possible to achieve a perfect match. A true Faraday rotation isolator with low loss would have been the ideal solution to the isolation problems for harmonic and fundamental resonance.

The purpose of the lenses L_1 and L_2 shown in Fig. 8 was to match the fundamental beam from the laser to the external harmonic resonator and scanning Fabry-Perot resonator. When properly matched to a scanning Fabry-Perot [29] (in beam radius and phase front curvature), all the incident power couples to the lowest-order resonator mode. In the case of the harmonic resonator, we fed it with a fundamental beam of radius $\sqrt{2}$ times larger than the beam radius of the lowest order harmonic mode $w_2 = 0.017$ cm (see Table I), according to (13), and adjusted the beam minimum to be at the plane of the flat mirror of the plano-concave resonator. In spite of this matching, as we have already calculated for harmonic resonators with $\rho \neq 0$, double refraction causes coupling to the higher-order modes.

C. Lineup Technique

The technique for lining up the harmonic resonator was complicated by the use of two wavelengths, the combination of ordinary and extraordinary beams in the resonator, and the need to adjust the crystal angle for phase matching. The harmonic resonator was first adjusted for resonance, with the crystal only approximately adjusted in angle with an extraordinary wave 0.6328μ beam, for which the mirrors have about the same reflectivity as at 0.576μ . This was done first with lens L_1 removed and an isolator in place. The curved mirror M_1 was adjusted square to the beam, using smoke which made the beam trajectory visible enough to judge the coincidence of the incident and reflected beam at M_1 . Without touching the resonator, L_1 was inserted and positioned for resonance again. This assures that the lens has been introduced with its axis along the original beam axis. Thus, when the wavelength is changed to 1.15μ , the beam axis will not shift. Irises I_1 and I_2 are

used to reference the beam during the change to 1.15μ .

The final adjustment for phase matching was made at 1.15μ with M_2 removed. When reinserted, we expect harmonic resonance. If this fails, the entire lineup procedure can be repeated with an increasing chance of success. Crucial to this procedure is the fact that the beam was introduced at the curved mirror M_1 of the plano-concave resonator where the axes of the ordinary fundamental and the extraordinary harmonic are coincident (see Fig. 4). Final trimming adjustments were made visually by tilting the output mirror so as to coalesce the many harmonic beam reflections into a single spot which closely corresponds to optimum interaction with the lowest-order mode of the harmonic resonator.

V. EXPERIMENTAL RESULTS

In this section, we describe the results of experiments using the apparatus described in Section IV and show how they are interpreted in terms of Section II and III.

A. Harmonic Resonator Loss Measurements and Resolution

The loss per pass ϵ at 0.576μ , associated with the extraordinary wave for various harmonic resonator geometries, was deduced from measurements at 0.6328μ , where the mirror reflectivities are essentially the same; ϵ was found by using (34) and data of the type illustrated in Fig. 3.

Measurements with a plano-concave resonator with no crystal gave values of ϵ expected from the mirror reflectivities. However, for a plane-parallel resonator with no crystal, there was an additional 10 percent loss per pass beyond that expected from mirror reflectivities. This is probably due to slight inaccuracies in the piezoelectric scanner and mechanical instabilities associated with the long path used between laser and resonator (~ 1 m), both of which affect the plane-parallel geometry more seriously. Most work was done with the plano-concave resonator, in order not to incur the measured additional loss.

When a KDP slab was inserted into the plano-concave resonator, there was an additional 12 percent loss per pass beyond that expected from mirror reflectivities and bulk absorption; 8 percent comes from the dielectric discontinuity; the other 4 percent we attributed to surface imperfections. With a crystal cut at the Brewster angle, the loss per pass dropped ~ 9 percent, which still left an additional 3 percent to be accounted for by surface imperfections. The lowest loss arrangement and the one used for the actual harmonic resonance measurement involved attaching a pair of 1 mm-thick antireflection-coated quartz plates to a 1.23 cm-long KDP crystal with index matching fluid. This reduced surface reflections to less than 0.1 percent, but introduced ~ 0.4 percent transmission loss for both surfaces. This crystal in a plano-concave resonator with 99 percent mirrors gave a measured value of $\epsilon \sim 0.04$, or 4 percent, which is reasonable, considering the bulk absorption.

Figure 9 illustrates the resolution possible with the

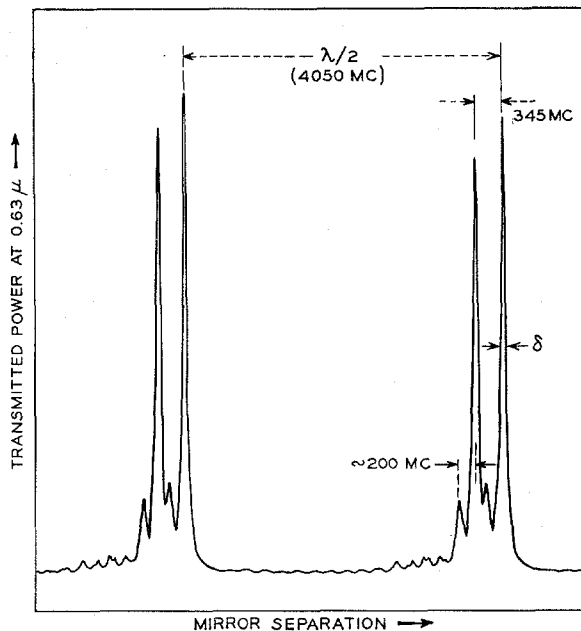


Fig. 9. Response of the plano-concave harmonic resonator to 0.6328μ light consisting of two longitudinal modes ~ 345 mc apart. The principal response is in the TEM_{00} mode of the resonator. A weaker response in the TEM_{10} mode displaced ~ 200 mc away from each of the two TEM_{00} modes is also illustrated.

plano-concave resonator containing the KDP sample clad with the two antireflection-coated quartz plates. It is also typical of the loss measurements. This data was taken with M_1 a 99 percent 1 m curved mirror, and M_2 a 97 percent flat mirror. The laser was 42 cm long, oscillating at 0.6328μ in the extraordinary wave. The figure shows the resonant response of the external resonator as it is scanned in length. Every time $c/2d'_e = 4050$ mc [see (63)], we expect the resonances to repeat. This corresponds to moving the mirror M_2 a distance of $\lambda/2$. Since the piezoelectric mirror drive on M_2 is linear, it conveniently provides an abscissa on Fig. 9 which is linear in frequency, from which we deduce that the 0.6328μ laser was oscillating in two well-resolved modes, ~ 345 mc apart. From the laser length, we expect longitudinal modes spaced every 360 mc. The ratio $\lambda/2\delta$ yields a value of $\epsilon = 0.5$, as expected from the earlier discussion.

Figure 9 also shows another feature of the harmonic resonator which will be important in the interpretation of the harmonic resonance data. This is the presence of the small satellite resonance ~ 200 mc away from each large resonance. These are due to the TEM_{10} mode of the resonator. In this case, this mode is being excited because of residual beam misalignment or slight errors in the beam-matching conditions. The mirror separation d at which the various TEM_{mna} modes of a plano-concave resonator in vacuum (or air) are resonant is given by Boyd and Kogelnik [13], eq. 48

$$\frac{2d}{\lambda} = q + \frac{1}{2\pi} (1 + m + n) \cos^{-1} \left(1 - \frac{2d}{b_1} \right) \quad (67)$$

where b_1 is the radius of the curved mirror, and m , n , and q are integers appropriate to the mode under con-

sideration. For a resonator partially filled with dielectric, we use $d = d'_e$ [see (63)] on the left-hand side of (67). On the right-hand side in the \cos^{-1} term, we use $d = d_e$ [see (61)]. For our resonator $b_1 = 1$ m and $d_e = 2.53$ cm. From (67), the difference in mirror separation between the TEM_{00a} and TEM_{10a} resonances is $\lambda/2\sqrt{d_e/b_1}$, which corresponds to ~ 204 mc. This agrees with Fig. 9. We emphasize that the 204 mc separation between the TEM_{00a} and TEM_{10a} modes, as used here, is merely a convenient way of quoting the mirror separation between transverse modes of the same frequency.

Since we expect essentially the same Q and resolution when looking at harmonic resonance at 0.576μ as at 0.6328μ [see (31) and (34)], we conclude that the Q is adequate in this resonator to resolve the harmonics of the longitudinal modes of the 1.15μ fundamental oscillator. As we shall see, we can also resolve the sum frequencies of the various longitudinal modes.

B. Harmonic Resonance

A convenient condition for observing the harmonics and mixing of axial modes is achieved by using a relatively short 1.15μ laser oscillating in two longitudinal modes of equal amplitude having frequencies f_1 and f_2 , spaced by $\Delta f = f_2 - f_1 \cong c/2L$. We then expect an output at three frequencies $2f_1$, $f_1 + f_2$, and $2f_2$, having relative powers 1, 4, 1, respectively, spaced by Δf . If the length of the laser tube L is increased, the number of oscillating modes increases and their separation decreases. This reduces the separation of the harmonic and sum components and makes their resolution in the external resonator more difficult. Suppose, for example, we have four fundamental longitudinal modes spaced by $c/2L$, as shown in Fig. 10(a), with frequencies f_1 , f_2 , f_3 , and f_4 . We expect an output of harmonic and mixed components at seven output frequencies, as shown in Fig. 10(b). The central three output modes are made up of two contributions each. For instance, output at $2f_2$ consists of the second harmonic of f_2 at $2f_2$ and $f_1 + f_3 = 2f_2$, taken in proper phase. In actual lasers, dispersion and saturation effects result in a spectrum of longitudinal modes slightly different from $c/2L$, with each mode having a phase independent of its neighbors [30]. These small shifts in spacing split the degeneracy of each of the central three modes of Fig. 10, so that, in fact, we have three closely-spaced doublets and a total of ten different output frequencies. In our apparatus, these closely-spaced pairs would not be resolved. With higher numbers of longitudinal modes oscillating, the output would consist of even larger numbers of unresolved lines, spaced approximately $c/2L$. Fluctuations in the laser mirror spacings, gas discharge, and small amounts of coupling back from the external resonator also give rise to amplitude and frequency fluctuations in the laser modes. These effects complicate the multimode situation and contribute to the observed instabilities under these conditions.

It is important to note that Fig. 10(b) describes only

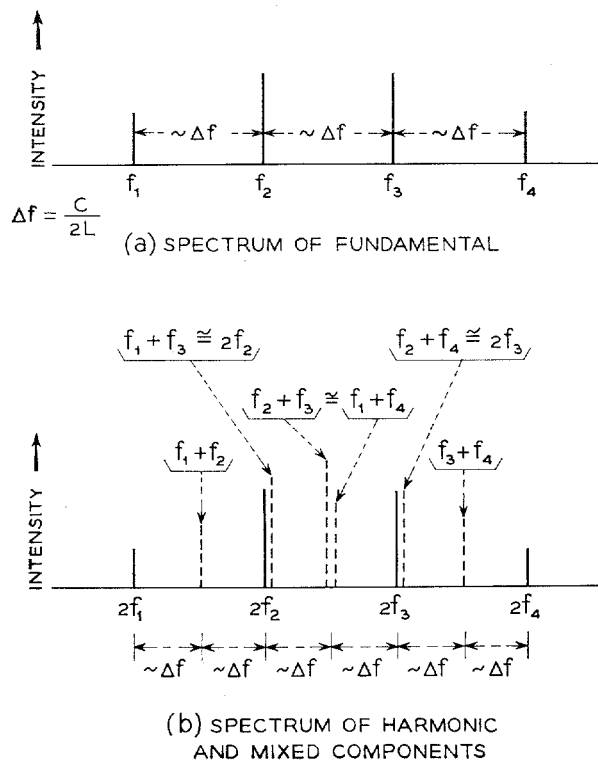


Fig. 10. Spectrum of harmonic and mixed frequency components generated by four equally-spaced fundamental longitudinal modes.

the frequency spectrum of the harmonic output. This output couples predominantly to the TEM_{00} mode of the harmonic resonator and, to a lesser extent, to the TEM_{10} mode and other higher-order modes. Thus, for each frequency present, there will be a series of resonances of decreasing amplitude, each of which occurs at a different value of the mirror separation, as determined by (67).

Figure 11 shows the laser output from a $L = 42$ cm tube oscillating at 1.15μ , as monitored by the scanning Fabry-Perot. The tube is oscillating in two longitudinal modes with somewhat unequal amplitudes, spaced ~ 360 mc $\cong c/2L$. The harmonic power output P_t from these two modes is shown in Fig. 12 as a function of the mirror separation of the plano-concave resonator, with mirror reflectivities $M_1 = 98.8$ percent and $M_2 = 97$ percent. We see successive groups of resonances spaced $\sim c/2d'_e \cong 4050$ mc, from which we deduce that the separation between the most prominent resonances of each group is ~ 340 mc. Thus, referring to Fig. 10(b), we conclude that we must be observing the sum frequency as well as the harmonics of the two incident longitudinal modes. The poorly resolved structure of Fig. 12, which constitutes the high base from which the three dominant resonances emerge, is taken as evidence of the higher-order modes. It is typical of these harmonic resonance measurements that the successive groups of resonances are not completely identical.

By comparing P_t at the peak of the central resonance (65 units of power) with the single-pass power obtained by removing the rear mirror M_2 of the resonator (12 units of power), we get a measure of the power enhance-

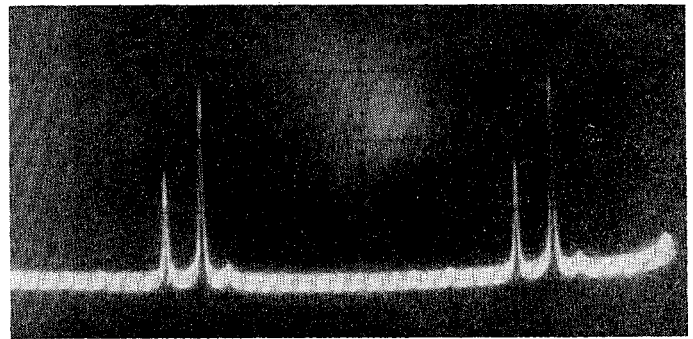


Fig. 11. Laser output from a $L = 42$ cm tube as monitored on the scanning Fabry-Perot. The two modes at $\sim 1.15 \mu$ are spaced ~ 360 mc $\cong c/2L$.

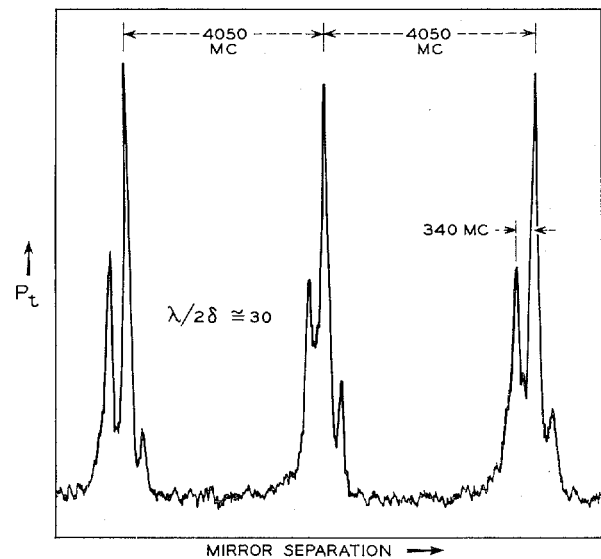


Fig. 12. Harmonic output P_t from the harmonic resonator vs. mirror separation for $L = 42$ cm. The principal response consists of three resonances spaced ~ 340 mc apart $\cong c/2L$.

ment factor P_t/P_e in (27). From the relative amplitude of the harmonic components seen in Fig. 12, we deduce that the single-pass power in the central resonance is $\sim .6 \times (12 \text{ units})$, or 7.2 units of power. Therefore, $P_t/P_e = 65/7.2 = 9.0$ (measured) for the central resonance. We compare this factor with the theoretical value computed from (27), making the assumption that only the lowest-order Gaussian mode of the resonator is excited. Thus, $\kappa = 0.43 = c_{a0}^2$ for $l/l_a = 0.87$ (see Table I and Fig. 5). Also, $\epsilon = 0.05 = (1 - r)$ and $t_2 = 0.03$, which gives $P_t/P_e = 5.2$ (calculated). From (31), $\lambda/2\delta = 63$ (calculated), whereas $\lambda/2\delta \cong 30$ (measured). From (24), setting $\varphi = 0$, we deduce that the resonant enhancement factor for harmonic power inside the resonator is $1/t_2$ times the enhancement factor for transmitted power (27). Thus, internal to the resonator, we have an enhancement of $P_e/P_e = 9.0/0.03 = 300$ (measured). These results, using the $L = 42$ cm laser, are summarized in Table II.

With $L = 64$ cm, the laser oscillated predominantly in four longitudinal modes, separated by about 235 mc. The harmonic resonator output consisted of about seven

TABLE II

	ϵ measured	P_t/P_2 measured	P_t/P_2 calculated	P_e/P_2 measured	P_e/P_2 calculated	$\lambda/2\delta$ measured	$\lambda/2\delta$ calculated
$L = 42$ cm	0.05	9.0	5.2	300	173	~ 30	63
$L = 64$ cm	0.04	—	—	—	—	~ 40	79
$L = 145$ cm	0.04	~ 7.0	3.2	~ 580	266	~ 40	79

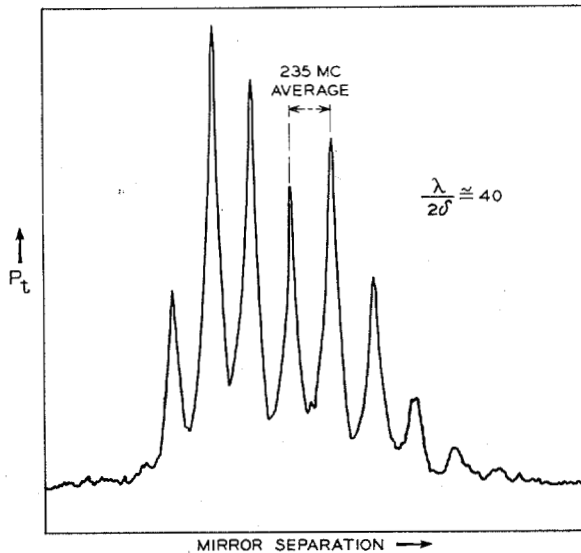


Fig. 13. Harmonic resonator output P_t from a 1.15μ laser with $L = 64$ cm oscillating mainly in four longitudinal modes separated by ~ 235 mc.

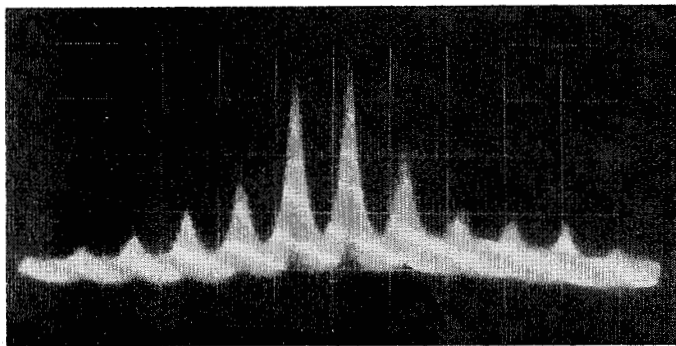


Fig. 14. Multiple exposure photograph of the laser output spectrum at 1.15μ for $L = 145$ cm. The spacing of modes is ~ 103 mc. The laser discharge was oscillating at ~ 400 Kc.

clearly resolved resonances, separated by 235 mc, as seen in Fig. 13. These resonances are more closely spaced than the resonances of Fig. 12, and yet appear better resolved. The reason is probably associated with the fact that the separation in position of the various transverse modes of a given frequency corresponds to ~ 204 mc, which is close to the 235 mc separation between sum and mixed frequency components. Thus, each resolvable resonance represents the sum of a TEM_{00} response at one frequency, and a TEM_{10} response of a neighboring frequency $c/2L = 235$ mc away, and possibly even some lesser contributions from other transverse modes at

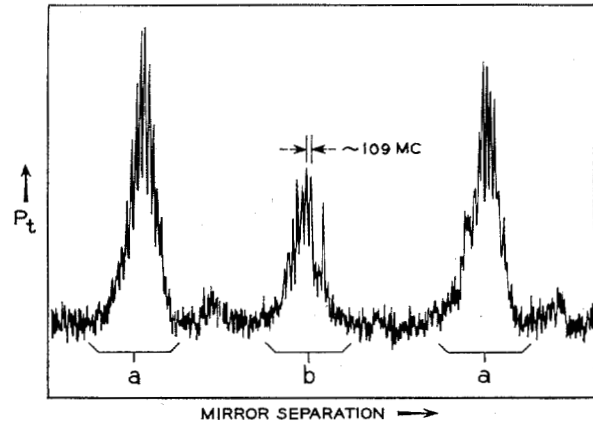


Fig. 15. Response of the harmonic resonator P_t to the incident fundamental light from the $L = 145$ cm laser, as a function of the mirror separation of the harmonic resonator.

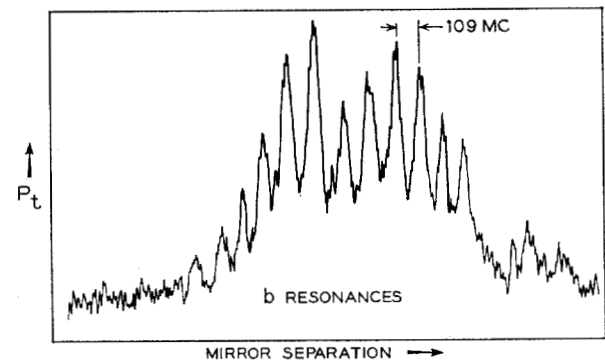


Fig. 16. Response of the harmonic resonator with an expanded scale showing the b resonances of Fig. 15 in detail.

still more remote frequencies. In this experiment, M_1 and M_2 had reflectivities of 98.8 percent. The value of $\lambda/2\delta$ increased somewhat to ~ 40 , consistent with the higher Q .

Data was also obtained from a laser with $L = 145$ cm, having a 103 mc longitudinal mode spacing. Figure 14 is a photograph of the output spectrum at 1.15μ . The harmonic resonator with two 98.8 percent mirrors gave harmonic output P_t , as shown in Fig. 15, with a separation of resonances of about 109 mc. Figure 16 shows data on the b resonances taken on an expanded scale. The situation here is similar to that of Fig. 13. Each resonance represents, principally, the response to the TEM_{00} mode and, to a lesser extent, the TEM_{10} mode having a frequency which is now $2(c/2L) = 206$ mc

away, plus some smaller higher-order mode contributions. The ratio of the output power P_t at the peak of the highest b resonance to the single-pass power with the output mirror removed was unity. From the fraction of the single-pass power in the highest b resonance, we deduce the enhancement ratios shown in Table II. The table also shows the measured value of $\lambda/2\delta$ and the comparisons with theory, assuming again that coupling occurs only to the lowest-order Gaussian mode.

The alternation in the amplitude of successive groups of resonances observed in Fig. 15 was ascribed to a chance coincidence of the harmonic resonance and the fundamental resonance caused by the residual reflections of the mirrors at 1.15μ . This coincidence does not always occur, due to the dispersion of the quartz plates, index fluid, and mirrors. It is interesting to note that the 145 cm tube was operating with a discharge oscillation at 400 kc. This affected the amplitude of the modes, as seen on the scanning Fabry-Perot. The Fig. 14 photograph was taken with a long exposure time and represents an average over a great many sweeps. Apparently, this oscillation did not adversely affect the resonator output, as seen in Fig. 15. In fact, similar data on tubes of comparable length which were free of oscillations showed somewhat greater variations in the heights of successive resonances. Possibly, the oscillation inhibited any locking of the modes to each other or to the external resonator.

In Table II, the comparisons between the measurements and calculations based on the excitation of only the lowest-order Gaussian mode show that the calculated values of the power enhancement are too low, and the calculated resonant width too narrow.

These discrepancies, which are at most a factor of two, can be reduced at certain places in Table II by including the coupling to the TEM_{10} and other higher-order modes. Thus, at $L = 145$ cm (data of Figs. 15 and 16), the inclusion of the coupling c_{21}^2 to the TEM_{10} mode (see Fig. 5) would increase P_t/P_2 calculated and P_e/P_2 calculated by a factor of $(c_{20}^2 + c_{21}^2)/c_{20}^2 \cong 1.6$. The extent of the contribution of the higher-order mode couplings at $L = 42$ cm (data of Fig. 12) is less clear, although these modes may be causing an overestimate of the measured value of δ . The agreement between experiment and theory in Table II is considered satisfactory. The complication of higher-order modes could have been eliminated, at the price of a little additional loss, by adding an iris of appropriate diameter to the harmonic resonator. In our short resonator, with its small spot size, this was difficult, and therefore was not done. There was direct evidence of coupling to the higher-order modes from visual observation of the resonant harmonic light. At optimum mirror alignment, there always was a residual halo about the central spot, predominantly elongated in the x direction, which indicates the presence of the TEM_{10} and other higher-order modes.

In the harmonic experiments described, the geometry

used was a compromise between the need for adequate signal-to-noise level at the detector, the desire to have a sample of sufficient length to display the effects of double refraction, and the need for adequate Q to resolve the longitudinal modes of the laser. No real attempt was made at optimization.

Keeping within the near-field restriction ($\xi_{KDP} \ll 1$), we see from (27) that considerable improvements in resonant power are still possible. Reducing l and w_2 in the same ratio decreases $\epsilon = (1 - r)$ and keeps κ and P_2 fixed, and thus increases P_t . Depending on ϵ , a reduction in l may increase κ/ϵ^2 more than it reduces P_2 , and thus increase P_t .

C. Fundamental Resonance

We will consider our data on resonance of the fundamental, taken with the external resonator equipped with two plane mirrors, coated to give high reflectivity at 1.15μ and high transmission at the harmonic wavelength. The input mirror M_1 was of variable reflectivity, as previously described for matching purpose. M_2 had a reflectivity of 99.5 percent at 1.15μ . The sample used was a 3.5 mm thick KDP crystal, cut at the Brewster angle for the fundamental. The previous results on loss per pass for a plane-parallel resonator with no sample showed 10 per cent more loss per pass than could be accounted for by the mirrors. This in itself is an indication that the results which include the sample will be considerably degraded. It was found that it was not possible to achieve a perfect match at resonance by varying the input mirror reflectivity. The reflected power went through a broad minimum of ~ 30 percent of the incident power for an input mirror reflectivity of 0.89. Also, as expected for this resonator, the response of the detected harmonic light as the fundamental goes through resonance (seen in Fig. 17) is rather broad, and yields a loss per pass $\epsilon = 0.28$. Taking 5 percent loss for the bulk absorption of the fundamental, 3 percent loss due to imperfections in the Brewster surface, $5\frac{1}{2}$ percent for the known mirror reflectivities, and 10 percent additional loss for the plane parallel resonator in our setup, accounts for $23\frac{1}{2}$ percent of the 28 percent observed.

From the measured $\epsilon = 0.28$ and the mirror reflectivities, we compute an effective value of the transmission through the nonlinear material $t = 0.77$. Substituting in (51) and (56), we find that the power at the input of the crystal inside the resonator at resonance $P_{em} = 1.6 P_1$. Thus, we expect an enhancement of harmonic output of $(1.6)^2 = 2.6$ at resonance, compared with the single-pass power generated in the absence of resonance. The enhancement was measured experimentally by removing mirror M_1 , which subjects the crystal to the incident power P_1 . The experimental value of enhancement found was 5. This agreement must be considered fair, especially since we are applying a theory which assumes a perfect resonator to a situation where we strongly suspect that beam walkoff is the origin of the additional

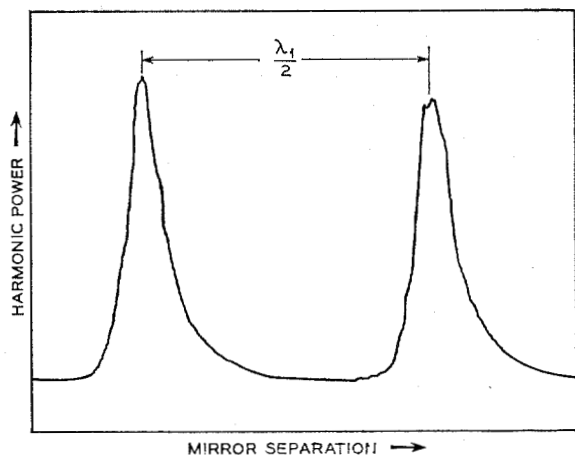


Fig. 17. Harmonic output from a plane parallel resonator containing *KDP*, which is tuned for resonance of the incident fundamental light.

unaccounted loss and the inability to achieve a perfect match. Had a perfect match been achieved with no additional loss at $r_1 = r_m = 0.89$, we would have expected a harmonic enhancement, from (56), of $1/(1 - r_m)^2 = 121$.

VI. SUMMARY

The use of optical resonance as a means of enhancing the efficiency of second-harmonic generation and frequency mixing in nonlinear crystals has been investigated experimentally and theoretically. This included resonance of the incident fundamental light at 1.15μ and also the generated harmonic light at $.576 \mu$. A plano-concave harmonic resonator containing *KDP* had an overall loss per pass of ~ 4 percent and adequate Q to resolve the harmonics and sum frequency components of the individual modes of the incident fundamental laser light. Large resonant enhancements were observed. The harmonic power internal to the resonator could be increased by ~ 500 times and external to the resonator by ~ 10 times. Clear resonant effects were observed when resonating the fundamental in a plane-parallel resonator, and an enhancement of 5 was seen. The results make it clear that the optimum signal sources for resonant nonlinear effects are in a single transverse and longitudinal mode.

A theoretical calculation of the expected enhancements due to resonance was presented, including the specific transverse energy distributions of the incident and generated light beam which gives rise to coupling factors to the relevant resonator modes. Satisfactory agreement between experiment and theory was obtained, using the measured optical loss for the resonators. The results suggest that further extensions of the experimental technique can lead to even larger enhancements in harmonic resonance, and especially in fundamental resonance using *KDP* or *LiNbO₃* phase matched normal to the optic axis.

This study, although specific to SHG and mixing, has direct theoretical and experimental relevance to

parametric oscillators. The resonance technique as used here for the second-order nonlinear polarization coefficient may be useful in the measurement of other weaker nonlinear interactions which, at present, are beyond the range of single-pass measurements.

ACKNOWLEDGMENT

The authors are grateful to J. P. Gordon for the benefit of numerous stimulating discussions, and to A. N. Chester, D. A. Kleinman, and R. G. Smith for critical reading of the manuscript.

REFERENCES

- [1] P. A. Franken, A. E. Hill, C. W. Peters, and G. Weinreich, "Generation of optical harmonics," *Phys. Rev. Lett.*, vol. 7, pp. 118-119, August 1961.
- [2] J. A. Giordmaine, "Mixing of light beams in crystals," *Phys. Rev. Lett.*, vol. 8, pp. 19-20, January 1962.
- [3] P. D. Maker, R. W. Terhune, M. Nisenoff, and C. M. Savage, "Effects of dispersion and focusing on the production of optical harmonics," *Phys. Rev. Lett.*, vol. 8, pp. 21-22, January 1962.
- [4] J. A. Armstrong, N. Bloembergen, J. Ducuing, and P. S. Pershan, "Interactions between light waves in a nonlinear dielectric," *Phys. Rev.*, vol. 127, pp. 1918-1939, September 1962.
- [5] N. Bloembergen and P. S. Pershan, "Light waves at the boundary of nonlinear media," *Phys. Rev.*, vol. 128, pp. 606-622, October, 1962.
- [6] D. A. Kleinman, "Theory of second harmonic generation of light," *Phys. Rev.*, vol. 128, pp. 1761-1775, November 1962.
- [7] G. D. Boyd, A. Ashkin, J. M. Dziedzic, and D. A. Kleinman, "Second-harmonic generation of light with double refraction," *Phys. Rev.*, vol. 137, pp. A1305-A1320, February 1965.
- [8] D. A. Kleinman, A. Ashkin, and G. D. Boyd, "Second harmonic generation of light by focused laser beams," to be published in *Phys. Rev.* vol. 145, pp. 338-379, May 1966.
- [9] A. Ashkin, G. D. Boyd, and J. M. Dziedzic, "Observation of continuous optical harmonic generation with gas masers," *Phys. Rev. Lett.*, vol. 11, pp. 14-17, July 1963.
- [10] N. I. Adams and P. B. Schoefer, "Continuous optical harmonic generation," *Appl. Phys. Lett.*, vol. 3, pp. 19-21, July 1963.
- [11] S. L. McCall and L. W. Davis, "Observation of continuous-wave optical harmonics," *J. Appl. Phys.*, vol. 34, p. 2921, September 1963.
- [12] G. D. Boyd and J. P. Gordon, "Confocal multimode resonator for millimeter through optical wavelength masers," *Bell Sys. Tech. J.*, vol. 40, pp. 489-508, March 1961.
- [13] G. D. Boyd and H. Kogelnik, "Generalized confocal resonator theory," *Bell Sys. Tech. J.*, vol. 41, pp. 1347-1369, July 1962.
- [13] G. D. Boyd and H. W. Kogelnik, "Generalized confocal resonator theory," *Bell Sys. Tech. J.*, vol. 41, pp. 1347-1369, July 1962.
- [14] G. D. Boyd, R. C. Miller, K. Nassau, W. L. Bond, and A. Savage, "*LiNbO₃*: an efficient phase matchable nonlinear optical material," *Appl. Phys. Lett.*, vol. 5, pp. 234-236, December 1964.
- [15] R. C. Miller, G. D. Boyd, and A. Savage, "Nonlinear optical interactions in *LiNbO₃* without double refraction," *Appl. Phys. Lett.*, vol. 6, pp. 77-79, February 1965.
- [16] S. A. Akhmanov, A. I. Kovrigin, R. V. Khokhlov, and O. N. Chunaev, "On the coherence length for waves interacting in nonlinear media," *Zh. Eksp. i Teoret. Fiz.*, vol. 45, p. 1336, 1963.
- [17] S. A. Akhmanov and R. V. Khokhlov, *Problems of Nonlinear Optics* (in Russian). AN SSSR, 1964.
- [18] R. H. Kingston and A. L. McWhorter, "Electromagnetic mode mixing in nonlinear media," *Proc. IEEE*, vol. 53, pp. 4-12, January 1965.
- [19] J. K. Wright, "Enhancement of second harmonic power generated by a dielectric crystal inside a laser cavity," *Proc. IEEE*, vol. 51, pp. 1663, November 1963.
- [20] R. G. Smith, K. Nassau, and M. F. Galvin, "Efficient continuous optical second harmonic generation," *Appl. Phys. Lett.*, vol. 7, pp. 256-258, November 1965.
- [21] A. Ashkin, G. D. Boyd, and D. A. Kleinman, "Phase-matched second-harmonic generation in *KDP* without double refraction," *Appl. Phys. Lett.*, vol. 6, pp. 179-180, May 1965.
- [22] R. H. Kingston, "Parametric amplification and oscillation at optical frequencies," *Proc. IRE*, vol. 50, p. 472, April 1962.

- [23] N. M. Kroll, "Parametric amplification in spatially extended media and application to the design of tuneable oscillators at optical frequencies," *Phys. Rev.*, vol. 127, pp. 1207-1211, August 1962.
- [24] C. C. Wang and G. W. Racette, "Measurement of parametric gain accompanying optical difference frequency generation," *Appl. Phys. Lett.*, vol. 6, pp. 169-171, April 1965.
- [25] J. A. Giordmaine and R. C. Miller, "Tuneable coherent parametric oscillation in $LiNbO_3$ at optical frequencies," *Phys. Rev. Lett.*, vol. 14, pp. 973-976, June 1965.
- [26] H. W. Kogelnik, "Coupling and conversion coefficients for optical modes," *Proc. Symposium on Quasi-Optics*, Brooklyn, N. Y.: Polytechnic Press, 1964, vol. 14, pp. 333-347.
- [27] A. J. Rack and M. R. Biazzo, "A technique for measuring small optical loss using an oscillating spherical mirror interferometer," *Bell Sys. Tech. J.*, vol. 43, pp. 1563-1579, July 1964.
- [28] H. Kogelnik, "Imaging of optical modes—resonators with internal lenses," *Bell. Sys. Tech. J.*, vol. 44, pp. 455-494, March 1965.
- [29] R. L. Fork, D. R. Herriott, and H. W. Kogelnik, "A scanning spherical mirror interferometer for spectral analysis of laser radiation," *Appl. Optics*, vol. 3, pp. 1471-1484, December 1964.
- [30] W. R. Bennett, Jr., "Hole burning effects in a He-Ne optical maser," *Phys. Rev.*, vol. 126, pp. 580-593, April 1962.
- [31] G. D. Boyd and A. Ashkin, "Theory of parametric oscillator threshold with single mode optical masers and observation of amplification in $LiNbO_3$," *Phys. Rev.*, vol. 146, pp. 187-198, June 1966.

Laser Bibliography III

Compiled by

K. TOMIYASU, FELLOW, IEEE

Abstract—This laser bibliography, compiled during the period from July through December, 1965, contains 644 references which are divided into 25 subject categories and listed chronologically. Brief annotations are added to many references.

THIS BIBLIOGRAPHY of 644 references was compiled during the period from July through December, 1965, and follows those published in the June and August, 1965, issues of IEEE JOURNAL OF QUANTUM ELECTRONICS. The references are divided into 25 categories and are listed in chronological order. A few of the references are dated prior to the compilation period. Brief annotations are added to many references. Some of the references are listed under more than one subject category because of the contents of the paper.

The subject categories and their scope are the same as those of *Laser Bibliography II*, except "Beam Quality" has been added to category 17. Twenty-seven references dealing with holograms are listed under category 24.

The subject categories are listed below, and the number of references in each category is given in parentheses.

- 1) Books and General Laser Papers (13)
- 2) Laser Analyses (19)
- 3) Ruby Laser (34)
- 4) Neodymium Laser (18)
- 5) Other Solid-State Lasers (16)
- 6) He-Ne Gas Laser (25)
- 7) Other Gas Lasers (45)
- 8) Organic and Chemical Lasers (1)
- 9) GaAs and $GaAs_{1-x}P_x$ Injection Luminescent Devices (31)
- 10) Other Injection Luminescent Devices and Analyses (7)

- 11) Laser Amplifier (12)
- 12) Laser Resonators and Mode Considerations (45)
- 13) Giant Pulse Techniques (*Q*-Switching) (16)
- 14) Pumping, Light Sources, Sensitization, and Population Inversion (15)
- 15) Modulation (25)
- 16) Detection (16)
- 17) Beam Quality, Control, and Steering (17)
- 18) Coherence, Interference, Quantum Noise, Narrow-Linewidth Lasers, and Frequency Control (33)
- 19) Raman and Brillouin Scattering (25)
- 20) Harmonic Generation, Mixing, and Other Parametric Interactions (22)
- 21) Thomson Scattering, Compton Scattering, and Plasma Diagnostics (12)
- 22) Other Nonlinear, Thermal, and Interaction Effects with Matter (42)
- 23) Transmission, Propagation, Scattering, Reflection, and Filtering (63)
- 24) Applications: Current and Proposed (59)
- 25) Miscellaneous (33)

1. BOOKS AND GENERAL LASER PAPERS

Nonlinear Optics

N. Bloembergen (Harvard U.)

W. A. Benjamin, Inc., New York, N. Y., 222 p., 1965 (general treatment, experimental results)

Nonlinear Optical Phenomena

Paul N. Butcher

Ohio State U., Engineering Experiment Station, Bulletin 200, 143 p., 1965 (Ohio State U. Seminar lecture notes)

Coherence Properties of Optical Fields

L. Mandel and E. Wolf (U. of Rochester)

Rev. Mod. Phys., Vol. 37, No. 2, pp. 231-287, April 1965 (extensive review, coherence effects, superposition effects, numerous references)